Microsystem Technologies

PDMS MICROFLUIDICS DEVELOPED FOR POLYMER BASED PHOTONIC BIOSENSORS

--Manuscript Draft--

Manuscript Number:	MITE-D-13-00072R3
Full Title:	PDMS MICROFLUIDICS DEVELOPED FOR POLYMER BASED PHOTONIC BIOSENSORS
Article Type:	Special Issue: Microfluidics 2012
Keywords:	photonic biosensor, microfluidics, PDMS surface modification, protein adsorption, TX-100, PDMS-PEO
Corresponding Author:	Péter Fürjes, Ph.D. HAS Research Centre for Natural Sciences Budapest, HUNGARY
Corresponding Author Secondary Information:	
Corresponding Author's Institution:	HAS Research Centre for Natural Sciences
Corresponding Author's Secondary Institution:	
First Author:	Péter Fürjes, Ph.D.
First Author Secondary Information:	
Order of Authors:	Péter Fürjes, Ph.D.
	Eszter Gabriella Holczer
	Eszter Tóth
	Kristóf Iván, Ph.D.
	Zoltán Fekete, Ph.D.
	Fabian Dortu, Ph.D.
	Domenico Giannone, Ph.D.
	Damien Bernier
Order of Authors Secondary Information:	
Abstract:	In this work, advances in the fabrication technology and functional analysis of a polymer microfluidic system - as a significant part of a developed polymer photonic biosensor - are reported. Robust and cost-effective microfluidics in PDMS including sample preparation functions is designed and realized by using SU-8 moulding replica. Surface modification strategies using Triton X-100 and PDMS-PEO and their effect on device sealing and non-specific protein adsorption are investigated by contact angle measurement and in situ fluorescence microscopy.
Response to Reviewers:	Dear Editors and Reviewers, First of all, thank You for the effort in improving our paper. Regarding the reviewer comments, we made the following modifications regarding the latest version of the manuscript submitted. The modifications and the required supplements are submitted in pdf format with the revised manuscript. Thank You again for the efforts to improve our manuscript. Regards, Péter Fürjes

PDMS MICROFLUIDICS DEVELOPED FOR POLYMER BASED PHOTONIC BIOSENSORS

P. Fürjes[1*], E. G. Holczer[1], E. Tóth[2], K. Iván[2], Z. Fekete[1], D. Bernier[3], F. Dortu[3], D. Giannone[3]

[1]Research Centre for Natural Sciences, Institute for Technical Physics and Materials Science, P.O.Box 49, H-1525 Budapest, Hungary
furjes.peter@ttk.mta.hu, holczer.eszter@ttk.mta.hu, fekete.zoltan@ttk.mta.hu
[2]Pázmány Péter Catholic University, Faculty of Information Technology and Bionics, H-1083 Budapest, Práter str. 50/a, Hungary
totes@digitus.itk.ppke.hu, ivan.kristof@itk.ppke.hu
[3]Multitel asbl, 2 rue Pierre et Marie Curie, 7000 Mons, Belgium
bernier@multitel.be, dortu@multitel.be, domenico.giannone@multitel.be

Corresponding author
Péter Fürjes
Research Centre for Natural Sciences, Institute for Technical Physics and Materials Science, H-1525 Budapest, P.O. Box 49, Hungary
Tel: +36 1 392 2616
Fax: +36 1 392 2235
E-mail: furjes.peter@ttk.mta.hu

KEY WORDS

photonic biosensor, microfluidics, PDMS surface modification, protein adsorption, TX-100, PDMS-PEO

ABSTRACT

In this work, advances in the fabrication technology and functional analysis of a polymer microfluidic system – as a significant part of a developed polymer photonic biosensor – are reported. Robust and cost-effective microfluidics in PDMS including sample preparation functions is designed and realized by using SU-8 moulding replica. Surface modification strategies using Triton X-100 and PDMS-PEO and their effect on device sealing and non-specific protein adsorption are investigated by contact angle measurement and in situ fluorescence microscopy.

* Corresponding author

1. INTRODUCTION

The main goal of P3SENS (FP7-ICT4-248304) project is to develop and realize a reliable point-of-care diagnostic device, which is applicable to detect blood protein markers of cerebro-vascular symptoms e.g. stroke with high sensitivity [1]. The proposed molecule sensing principle is based on the extremely sensitive detection of lightwave propagation change in nanostructured waveguides due to binding of molecules on their surface. The target molecules could be captured by special receptors previously deposited on the waveguide surfaces causing refractive index shift of the surrounding region where the evanescent field develops. [2] Our proposed biosensor addresses the integration of optical detection unit and sample preparation microfluidics into a single lab-on-a-chip system.

To reduce manufacturing costs both the optical and the microfluidic parts of the sensor are realized in widely used polymers like polyimide (PI) and poly-dimethylsiloxane (PDMS) by using nano-imprint-lithography (NIL) and soft lithography, respectively. PDMS [3] is a silicon based organic polymer: $(H_3C)_3[Si(CH_3)_2O]_nSi(CH_3)_3$ and is an attractive material of current bioanalytical microfluidics due to its easy and reliable pattern transfer, flexibility, transparency, biocompatibility, chemical and biological resistance and low cost [4, 5]. Besides challenges in mass production of PDMS microsystems [6, 7], the process compatibility with other polymers is still in the focus of ongoing researches on lab-on-a-chip applications [8]. The inherent hydrophobic surface property, non-specific molecule (e.g. protein) adsorption are key issues as regards reliability of microfluidic part of a PDMS-based sensor [5, 6, 7, 9]. On the other hand, the addition of surfactants can beneficially change the above properties [10]. Materials like TX-100 [11] and PDMS-PEO (poly(dimethylsiloxane-ethylene oxide polymer)) [12] has been successfully introduced to the fabrication of microfluidics for analytical purposes, however, the effect of their integration into a complex microsystem was not described so far.

In our work, hydrodynamic properties, the effect of surface modification on wettability and sealing of a polymer microsystem is investigated in details.

2. EXPERIMENTAL

2.1 Design

Our microfluidic system includes fluidic inlets and outlets, transport channels, embedded mixer structure and aligned optical parts as well. Design schematics and a cross-sectional drawing are shown in Figure 1.a and b. The optical microsystem to be bonded to the microfluidics contains a laser coupler, an optical waveguide running under the fluidic channels. The topology transferred to the PDMS substrate is represented by Figure 1.c.

2.2 Microfabrication

Polymer microfluidics was fabricated by PDMS soft lithography technique (as schematically illustrated by Fig. 2) utilizing multi-layered SU-8 epoxy based negative photoresist [13, 14, 15] as a master replica for PDMS moulding [3]. The SU-8 layers were patterned by subsequent spin-coatings and lithographic exposures and a final development step. Each layer contains different functional components of the microfluidic system. The first, bottom layer of SU-8 defines the fluidic channels with reservoirs and T-mixers, and the second layer includes fluidic inlets and the periodic relief of a herringbone mixer. Multi-layer moulding form for the examined herringbone chaotic mixer is shown in Figure 3. The PDMS raw material was blended and grafted by surfactant molecules (TX-100 and PDMS-PEO) applying their concentration range of 0-0.2 v/v%. The volumetric ratio of the elastomer and the curing agent was 10:1 as specified by the developer (Dow Corning, Sylgard® 184). The raw PDMS was moulded onto the developed moulding replica and polymerised in room conditions in two days. Then the cured PDMS was peeled and bonded onto the photonic chip surface.

In our project, the photonic chip is developed from nano-composite polymeric materials using highly scalable nano-imprint-lithography (NIL) [16]. The structured photonic waveguide was visualised by AFM as presented in Figure 4. To check bonding properties, a range of polymer materials has been used as substrate

for the optical parts. Reliability and long-term stability of adhesion between fluidic and optical units was examined using P84® polyimide [17] and SU-8 [13] as high refractive index (HRI) material, and poly(methyl methacrylate) (PMMA) and fluorinated materials as CYTOP® [18] as Low Refractive Index (LRI) material , respectively. Conventional MICROPOSIT 1818 photoresist [13] was used as reference. Several earlier reports presented bonding solutions with moderate adhesion between different polymers and PDMS applying subsequent O_2 or N_2 plasma treatments and possible silanisation steps utilising various organosilanes. [19, 20, 21, 22] These bonding experiments were reproduced and evaluated to find an optimal method to seal our photonic and microfluidic subsystems.

2.3 Surface modification

Polymers with hydrophilic chains and amphipathic molecules can be embedded in the bulk phase if added to the elastomer before polymerisation. After embedding, the hydrophobic group of the molecules interact with the hydrophobic PDMS, and the hydrophilic chain is interfaced by the liquid phase. This way the wettability of the surface can be increased. The molecules like shorter polymer chains can freely move in the bulk phase, therefore real hydrophilicity can only be achieved if interfaced by hydrophilic medium. This implies that good adhesion and surface modification can be performed simultaneously. In our work, the effect of tensides are investigated by embedding two different molecules (TX-100, PDMS-PEO), both containing hydrophilic poly-ethylene oxide, but having different hydrophobic group and size. The effect of both added tensides are investigated in the concentration range of 0-0.2 v/v%.

2.4 Measurements

To ensure the optimal fluidic performance of the microfluidic system, these basic functional units were analysed by FEM modelling and experimental investigations. Biological analytes (fluorescently labelled human serum albumin (HSA) buffered in PBS) were applied to verify the functionality [23, 24]. Due to the small characteristic dimension of microfluidic systems, the fluidic flows are laminar and the fluidic component streams are mixed by molecular diffusion, where a dynamically diffusive interface is created with predictable geometry. The mixing performance can be improved by generating chaotic advection which can cause secondary transversal transport and significantly improve mixing in the laminar flow regime. This implies that the use of smaller surface area microfluidic devices with slightly complex channel geometries is sufficient to achieve efficient mixing in the microscale [25, 26, 27].

The fluidic behaviour of three different mixer structures – herringbone type, staggered and simple T-mixers – were analyzed by Finite Element Modelling using COMSOL Multiphysics [28] solving Navier-Stokes and diffusion equations. The geometric parameters – especially in case of the herringbone type mixer – were also optimized.

The Navier-Stokes equation describes the fluidic motion of incompressible viscous liquids:

$$\rho\left(\frac{\partial v}{\partial t}+(v\nabla)v\right)=-\nabla p+\mu\nabla^2 v+f \qquad \text{(Eq.1)}$$

where $\boldsymbol{v}$ denotes the flow velocity, ρ is the density, p is the pressure, μ is the dynamic viscosity and $\boldsymbol{f}$ summarise the volumetric forces acting on the liquid (cca gravity).

The molecule concentration distribution was estimated by solving numerically the transport equation describing both the convection and diffusion phenomena:

$$\frac{\partial v}{\partial t}+v\nabla c=\nabla(D\nabla c) \qquad \text{(Eq.2)}$$

where c denotes the concentration and D is the diffusion coefficient.

To optimise the convergence of the numerical solution the mesh of the model was carefully defined, considering that the discretisation error may cause numerical diffusion which leads to the false mixing of species as presented in [29]. A free tetrahedral mesh was built joined with a boundary layer mesh along the no-slip boundaries. To ensure the usage of appropriate mesh resolution we conducted mesh convergence study by calculation the concentration fields applying subsequent mesh refinements. The concentration distributions at the outlet plane of the structure were chosen as convergence parameter. In each step the root mean square (RMS) of the difference between the concentration fields were calculated in case of the refined and the previous mesh. The final mesh resolution was accepted if the calculated RMS has reached the 8% criteria. The applied mesh consisted of tetrahedral (79,15%), pyramid (0,77%), prism (12,87%), triangular (7,19%) and quadrilateral elements (0,02%). Number of elements was 16.09.028. The mesh element sizes were between 1.25 µm and 6.6 µm in the free tetrahedral region, and 0.187 µm and 2.8 µm in the boundary region, respectively.

Initial boundary conditions were set to 0.1 mM/mL concentration of human serum albumin (HSA) solution and 2 µL/min aggregated flow rate in each model. The results of the simulations were verified by experimental flow characterization using fluorescent HSA diluted in phosphate buffered salt solution. The flow rate at the inlets was adjusted by injection pumps such that both the labelled HSA and the buffer solutions are introduced in equal distribution in the initial cross-section of the mixer structure. Since HSA proteins tend to bind to the channel walls, a pre-washing by bovine serum albumin (BSA) was applied. As a result, the hydrophobic bonds of the channel surfaces were completely blocked, which reduced noise on the fluorescent images significantly. The parameters of the above protocol are summarized in Table 2. Detected fluorescent intensity was then evaluated by image processing software ImageJ [30], which finally provided histograms corresponding with the concentration distribution of HSA solution in the examined cross-sections.

3. RESULTS & DISCUSSION

3.1 Fluidic functionality

The three micromixer structures were characterized by both modelling and experiments with special interest in chaotic advection effects. The calculated and recorded HSA distributions are summarized in Figure 5. The measured relative fluorescent intensities were illustrated and compared qualitatively to the modelled and vertically integrated concentration distributions at different cross-sectional plane of the structures. Both the numerical simulations and the experimental results showed the advantages of the double-layered herringbone structure in comparison with the staggered and the simple T-mixer structures. The results clearly proved that in the intermediate Reynolds number regime (1-100) the advective effect of the staggered blocks is not efficient enough and both the numerical and experimental results showed moderated mixing. The efficiency of the herringbone structures could be explained by the presence of anisotropic flow resistance in the channel and the generation of secondary flow-streams in the laminar regime. This transversal advection effect can be easily recognised by comparison of the concentration fields of subsequent cross-sectional planes.

Local minimum and maximum both in the vertically integrated concentration and in the fluorescent intensity appeared after the odd number of groove blocks in case of the herringbone structure. This periodic phenomena indicates the rotating effect of the anti-symmetrically formed groves and can be interpreted by the inclusion of a high concentration layer between the low concentration layers and vice versa. This effect could be recognised in both the experimental and the simulation results indicating a nice qualitative verification of our FEM model.

In the flow rate regime of 1-120 µL/min, the estimated Reynolds number is in the intermediate regime between 1-100. The square of the relative concentration deviation from the ideal value, $\Delta c^2_{relative}(x, y_0)$ clearly demonstrates the mixing state at various cross-sections of the mixer channel. By averaging the square of the relative concentration deviation along the cross-sections a general mixing efficiency parameter (*ME*) can be derived for each mixer structure as shown in Equation.3.

$$\Delta c^2_{relative}(x, y_0) = \left(\frac{c(x, y_0)}{c_{in}} - 0.5 \right)^2$$

$$ME(y_0) = \frac{\int_0^d \Delta c^2_{relative}(x, y_0) dx}{d} = \frac{\int_0^d \left(\frac{c(x, y_0)}{c_{in}} - 0.5 \right)^2 dx}{d} \quad \text{(Eq.3)}$$

and $\frac{\int_0^d c(x, y_0) dx}{d} = \frac{c_{in}}{2} = const.$

where x and y_0 represents the local coordinates in the channel at a given cross-section, c is the local and c_{in} is the maximal molecule concentration at the channel inlet, respectively, and w is the width of the channel.

The lowest *ME* values represent the most efficient mixing. In the applied intermediate Reynolds number regime, the characterized herringbone type mixer shows the best mixing efficiency in contrast to reference mixers like the staggered or the simple T-mixer as presented in Figure 6. Note that the mixing efficiency of the herringbone type mixer can be improved by applying odd number of blocks of grooves as confirmed in Figure 6 where the C4 line indicates $\Delta c^2_{relative}(x, y_0)$ function at the cross-sectional plane after the third block which is clearly beneficial compared to the state at the outlet plane after even number of the reflected anti-symmetrical blocks. The characterised cross-sections (C4 and outlet planes) are indicated in the micrographs of Figure 5.

Since the herringbone type mixer was chosen for further application and characterisation in the proposed microfluidic system the geometry of the mixer structure were optimised by Finite Element Modelling. The groove depth of the secondary relief structure was optimized particularly by the minimisation of the $\Delta c^2_{relative}(x, y_0)$ function calculated at the cross-sectional plane of the mixer outlet. The *ME* mixing efficiency parameters were also calculated in case of different ratio of relief depth and primary channel depth as demonstrated in Figure 7. The optimal depth of the groves was found to be in similar range with the primary channel height (20 µm), which is approximately 25-30 µm in our case.

3.2 Issues of bonding process

Since polyimide (PI) was selected as the optical material of the sensor, its bonding to PDMS was investigated in details. Adequate adhesion were achieved by subsequent silanisation (applying organofunctional alkoxysilanes as (3-aminopropyl)-triethoxysilane – APTES) processes and oxygen plasma treatments applied in the case of polyimide polymer surfaces as illustrated in Figure 8. For successful sealing we applied oxygen plasma activation (at the parameters of 1500 sccm O_2, 200 W, 180 s) of the polymer surface before silanisation. 5 v/v% solution of APTES was spin-coated and baked at the temperature of 85°C for 25 min. Note that the organosilane can be deposited by spin-coating process, since the polymer surface is structured in the nanoscale. If the polymer surfaces are structured in the microscale, organosilanes are to be deposited from the liquid or vapour phase instead of spin-coating. Just before the bonding the surfaces were also activated in oxygen plasma (at the parameters of 1500 sccm O_2, 200 W, 180 s).

The stability of the silanised and bare PI surface after plasma activation was characterized by a time dependent change of the water contact angle, as presented in Figure 9.

While the plasma activated polyimide surface can be slightly bonded to the PDMS substrate, the silanised and plasma activated surface can be reliably sealed with the PDMS fluidics within cca. 24 hours after the surface modification. This time window could be critical if the active part of the sensor has to be modified (e.g. considering the bio-functionalisation of the polyimide optical waveguide) before bonding to the microfluidics. PDMS counterpart of the device was treated by oxygen plasma as well. As regards, the effect of surfactant on substrate bonding we noticed that long term sealing occurs only below concentration 0.2 v/v% in case of both PDMS-PEO and TX-100, however, lower contact angles would be achieved [12] by applying higher additives concentrations.

3.3 Effect of surface modification on hydrophilicity

Apparent drawback of PDMS-based biosensors is the hydrophobicity of surfaces, which has a remarkable effect on the maximum flow rate in a microfluidic system. Moreover, the non-specific binding of proteins or ligands to the channel surface is also considerable due to the possible depletion of the target molecules transported to the active sensing area. TX-100 surfactant and PDMS-PEO were added to the raw PDMS before polymerisation. [31] The influence of the modification has been also studied and is found in literature [10, 11, 12, 32, 33]. Modified surface characteristics of our device were analyzed by contact angle measurement. Static contact angles are shown in Figure 10.

A significant change in water contact angle was observed in correlation with the embedded surfactant molecule concentration. The water contact angle of the PDMS achieved the hydrophilic region around 45° from the original value of 90° in case of 0.2 v/v% PDMS-PEO concentration. The developing surface behaviour can be explained by the accumulation of the embedded molecules at the PDMS surface. The rapidly decreasing contact angle during the measurement indicates the increasing surface concentration of the modifying molecules at the PDMS / liquid interface [33, 34, 35]. The long term stability of the developed molecule layers were reported more than months by [11, 12].

The improved wettability of the modified PDMS surface facilitates the design of fast capillary microfluidics. The characteristic capillary pressure in the channel system can be described by Equation 4:

$$P_c = -\gamma\left(\frac{\cos\alpha_b + \cos\alpha_t}{h} + \frac{\cos\alpha_l + \cos\alpha_r}{w}\right) \qquad \text{(Eq.4)}$$

where γ denotes the surface tension at the fluid/gas interface, $\alpha_{b/t/l/r}$ are the contact angles of the fluid at the channel *(bottom/top/left/right)* walls, and h and w are the height and the width of the channel, respectively. In our case, bottom surface of the channel was glass. Channel width was 100 µm, and height 50 µm. Change of wettability from hydrophobic to hydrophilic state (negative capillary pressure region) is represented by Figure 11.

We can conclude that both TX-100 and PDMS-PEO can significantly improve the surface wettability of the PDMS surface. Our experiments on PDMS-PEO also proved that lower concentrations (below 0.2 v/v%) than applied in literature [12] is suitable for relevant changes contact angles.

3.4 Effect of surface modification on protein binding

The non-specific adsorption of proteins on the exposed surfaces of the microfluidic channels is essential as regards bioanalytical tasks demanding high sensitivity [36]. To check our surface modified PDMS from this point of view, the adsorption of fluorescein-isothiocyanate (FITC) labelled HSA on the exposed channel surface was recorded by fluorescent microscopy. The irreversible protein adsorption on channel surfaces was evaluated by recording the relative fluorescent intensity of labelled HSA along the microchannel after subsequent washing by PBS as presented in Figure 12. The relative change in intensity after washing proved that irreversible HSA adsorption on the PDMS surface can be decreased by embedding 0.2 v/v% TX-100 or PDMS-PEO in the material. We can conclude that the irreversible protein adsorption on the PDMS surface can be decreased by almost 100% by this surface modification method [33].

The applied 0.2 v/v% embedded additive concentration ensures both the improved wettability and non-specific protein adsorption of the channel surfaces although it does not affect significantly the efficiency of the bonding process for the applied PI and PDMS materials.

4. CONCLUSIONS

This paper describes the technology and functional investigation of the microfluidic part of a polymer based optical biosensor. Microfluidics in PDMS was fabricated by soft lithography technique using SU-8 moulding replica. Several possible polymer bonding processes were validated and applied to make a leak-free adhesion between optical material (polyimide) and PDMS. Subsequent silanization of plasma treated PI proved to be a suitable preparation technique before alignment and bonding to PDMS microfluidics.

The functional performance of the microfluidic system was modelled by Finite Element Modelling and the results were verified experimentally. The mixing performance of the integrated herringbone and staggered T-type chaotic mixers were characterised and explained by the evolved transversal advection effects and the geometry of the herringbone mixer was optimised. Our results suggest that the mixing efficiency of the herringbone mixer is significantly improved, if odd number of blocks is applied.

Surface modification methods were also studied to improve both wettability and non-specific protein binding of PDMS. Triton X-100 surfactant and PDMS-PEO were added to the raw PDMS before polymerization. The influence of embedded molecules was analyzed in terms of contact angles and functionality. Contact angle of the modified PDMS surfaces was decreased by up to 30% and 50% in case of PDMS-PEO and TX-100 surfactant molecules, respectively, representing the significant change of the surface characteristics of the PDMS from hydrophobic to hydrophilic state. Moreover we found that irreversible protein adsorption on the PDMS surface can be decreased by almost 100% in both case. Eventually, we noticed that only low concentration of surfactants (below 0.2 v/v%) can be added without significantly deteriorating adhesion between PI and PDMS substrates.

ACKNOWLEDGEMENTS

The supports of the European Commission through the seventh framework program FP7-ICT4-P3SENS (248304) and the János Bolyai fellowship of the Hungarian Academy of Sciences (recipient: Péter Fürjes), also the support of the grants TÁMOP-4.2.1.B-11/2/KMR-2011-0002 and TÁMOP-4.2.2/B-10/1-2010-0014 is acknowledged. The significant efforts of M. Erős and M. Payer in microtechnology are gratefully acknowledged.

REFERENCES

[1] FP7 Framework Programme of European Commission: P3SENS, Polymer Photonic multiparametric SENSor for Point-of-care diagnostics, www.p3sens-project.eu

[2] X. Fan, I. M. White, S. I. Shopova, H. Zhu, J. D. Suter, Y. Sun, *Sensitive optical biosensors for unlabeled targets: A review*, Analytica Chimica Acta 620 (2008) 8–26

[3] Dow Corning Corp., www.dowcorning.com

[4] S. K. Sia, G. M. Whitesides, *Microfluidic devices fabricated in poly(dimethylsiloxane) for biological studies*, Electrophoresis 24, (2003) 3563–3576

[5] J. Cooper McDonald, D. C. Duffy, J. R. Anderson, D. T. Chiu, H. Wu, O. J. A. Schueller and G. M. Whitesides, *Fabrication of microfluidic systems in poly(dimethylsiloxane)*, Electrophoresis 21 (2000) 27-40

[6] A. Mata, A. J. Fleischman, and S. Roy, *Characterization of polydimethylsiloxane (PDMS) properties for biomedical micro/nanosystems*, Biomedical Microdevices 7 (4) (2005) 281-93

[7] J. Friend and L. Yeo, *Fabrication of microfluidic devices using polydimethylsiloxane*, Biomicrofluidics 4(2) (2010) 026502

[8] L. Gervais and E. Delamarche, *Toward one-step point-of-care immunodiagnostics using capillary-driven microfluidics and PDMS substrates*, Lab Chip 9 (2009) 3330-3337

[9] R. Mukhopadhyay, *When PDMS isn't the best*, Analitical Chemistry 79 (9) (2007) 3249-3252

[10] J. Zhou, A. V. Ellis, and N. H. Voelcker, *Recent developments in PDMS surface modification for microfluidic devices*, Electrophoresis 31 (1) (2010) 2-16

[11] J. Seo, and L. P. Lee, *Effects on wettability by surfactant accumulation/depletion in bulk polydimethylsiloxane (PDMS)*, Sensors and Actuators B 119 (2006) 192–198

[12] M. Yao and J. Fang, *Hydrophilic PEO-PDMS for microfluidic applications*, J. Micromech. Microeng. 22 (2) (2012)

[13] MicroChem Corp., www.microchem.com

[14] A. del Campo and C. Greiner, *SU-8: a photoresist for high-aspect-ratio and 3D submicron lithography – TOPICAL REVIEW*, J. Micromech. Microeng. 17 (2007) R81–R95

[15] A. Mata, A. J. Fleischman and S. Roy, *Fabrication of multi-layer SU-8 Microstructures*, J. Micromech. Microeng. 16 (2006) 276–284

[16] L. J. Guo, *Nanoimprint Lithography: Methods and Material Requirements*, Advanced Materials Vol. 19 4, (2007) 495–513

[17] Evonik Fibres GmbH, www.p84.com

[18] Cytec Industries Inc., www.cytec.com

[19] S. Talaei, O. Frey, P. D. van der Wal, N. F. de Rooij, and M. Koudelka-Hep, *Hybrid microfluidic cartridge formed by irreversible bonding of SU-8 and PDMS for multi-layer flow applications*, Procedia Chemistry 1 (2009) 381–384

[20] Vijaya Sunkara, Dong-Kyu Park, Hyundoo Hwang, Rattikan Chantiwas, Steven A Soper and Yoon-Kyoung Choa; *Simple Room Temperature Bonding of Thermoplastics and Poly(dimethylsiloxane)*, Lab on a Chip 11 (2011) 962

[21] Pengfei Li, Nan Lei, Debra A. Sheadel, Jie Xu, Wei Xue; *Integration of nanosensors into a sealed microchannel in a hybrid lab-on-a-chip device*, Sensors and Act. B 166 (2012) 870

[22] Jiheng Zhao, Debra A. Sheadel, Wei Xue; *Surface treatment of polymers for the fabrication of all-polymer MEMS devices*, Sensors and Actuators A 187 (2012) 43– 49

[23] N.-T. Nguyen and S. T. Wereley, *Fundamentals and applications of microfluidics,* Artech House, 2006

[24] N.-T. Nguyen, *Micromixers: fundamentals, design and fabrication*, William Andrew, 2008

[25] A. J. de Mello, *Control and detection of chemical reactions in microfluidic systems*, Nature 442 (2006) 394-402

[26] A. D. Stroock, S. K. W. Dertinger, A. Ajdari, I. Mezic, H.A. Stone and G.M. Whitesides, *Chaotic mixer for microchannels*, Science 295 (2002) 647–650

[27] J. H. E. Cartwright, M. Feingold, and O. Piro, *An introduction to chaotic advection*, *NATO ASI Series B Physics* 373 (1999) 307–342

[28] COMSOL Multiphyics, www.comsol.com

[29] V. P. Chua and O. B. Fringer, *Assessing the effects of numerical diffusion in a three-dimensional unstructured-grid model of a periodically-stratified estuary,* International Workshop on Multiscale Un-Structured Mesh Numerical Ocean Modeling, Cambridge, MA, U.S.A., August 2010.

[30] National Institute of Health, US Dept. Of Health and Human Services, rsbweb.nih.gov/ij/

[31] www.sigmaaldrich.com (TX-100: T8787 - CAS Number: 9002-93-1, PDMS-PEO: 482412 - CAS Number 68938-54-5)

[32] G. Sui, J. Wang, C.-C. Lee, W. Lu, S. P. Lee, J.V. Leyton, and A. M. Wu, *Solution phase surface modification in intact PDMS microfluidic channels*, Anal. Chem. 78 (2006) 5543-5551

[33] E. Holczer, Z. Fekete, P. Fürjes, *Surface modification of PDMS based microfluidic systems by tensides*, Material Science Forum 729 (2013) 361-366
[34] J. Kim, M. K. Chaudhury, and M. J. Owen, *The mechanism of hydrophobic recovery of PDMS elastomers exposed to partial electrical discharges*, J. Colloid Interface Sci. 244 (2001) 200-207
[35] S. Bhattacharya, Y. Gao, V. Korampally , M. T. Othman, S. A. Grant, K. Gangopadhyay, and S. Gangopadhyay, *Mechanics of plasma exposed spin-on-glass (SOG) and polydimethyl siloxane (PDMS) surfaces and their impact on bond strength*, Applied Surface Science 250 (2007) 4220–4225
[36] S. Ray, P. Jaipal Reddy, S. Choudhary, D. Raghu, S. Srivastava, *Emerging nanoproteomics approaches for disease biomarker detection: A current perspective*, J. of Proteomics 74 (2011) 2660-2681

BIOGRAPHIES

Péter Fürjes received his M.Sc. in Engineering Physics in 1999, his MBA in 2002 and Ph.D. degree in 2004 from Budapest University of Technology and Economics. He has been working in the field of silicon micromechanics and sensor technology for Tateyama Kagaku Ind. Co. (Toyama, Japan), Furtwangen University (Furtwangen, Germany) and Research Centre for Natural Sciences of the Hungarian Academy of Sciences, MTA TTK MFA (Hungary). He has been investigated operational, thermo-mechanical and fluid-dynamical behaviour of MEMS/NEMS devices. His current researches aim at design and analyse 3D heterostructures (silicon, glass and polymer) for analytical devices and micro- and nanofluidic applications, included modelling and realisation, together with development unique and novel micromechanical solutions and sensing principles. He is working for MTA TTK MFA as the head of BIOMEMS & Microfluidics Laboratory, and he is an invited lecturer of micromechanics and MEMS technology at the Budapest University of Technology and Economics.

Eszter Holczer received his B.Sc. in Chemical Engineering from the Budapest University of Technology and Economics in 2011. Since 2010, she is involved in polymer micromachining in the Research Centre for Natural Sciences (MTA TTK MFA), Budapest.

Zoltán Fekete graduated in electrical engineering from the Budapest University of Technology and Economics in 2009. He received his PhD in 2013 and currently he is a research fellow at the Institute of Technical Physics and Material Science of the Hungarian Academy of Sciences. His research interests include the development of MEMS devices, silicon and polymer microfluidics, and silicon-based neural microprobes.

Eszter Tóth received her MSc in info-bionics from Pázmány Péter Catholic University in 2014. She is currently a PhD student at the Research Centre for Natural Sciences of the Hungarian Academy of Sciences (MTA TTK MFA) in cooperation with the Pázmány Péter Catholic University. Her main interest is the finite element modeling of MEMS microfluidics by computational fluid dynamics.

Kristóf Iván received his MSc in bio-engineering from Budapest University of Technology and Economics in 2002, PhD in info-bionics from Pázmány Péter Catholic University in 2006. During his PhD he has been interested in nonlinear chemical sensors and MEMS devices. His current research is focused on microfluidic devices for blood analysis applications and digital microfluidic devices.

TABLE and FIGURE CAPTIONS

Table 1. Injection parameters of fluorescent measurements in the case of several solution.

Figure 1. Schematic cross-sectional view of the proposed biosensor (a) represents the architecture of the photonic and microfluidic part of the system. The functional blocks reflected the proposed sample preparation process (b.). The realised microfluidic structures are presented by the applied mask patterns of the multi-layer SU-8 moulding replica formation (c. and d.) (channel system: black layer, mixer system: gray layer).

Figure 2: Process flow for the fabrication of microfluidics.

Figure 3: Multi-layer SU-8 moulding master of herringbone chaotic mixer.

Figure 4: The AFM scan of the photonic chip presents the waveguide structure nanoimprinted in the polymer surface.

Figure 5: The measured (left) fluorescent intensity of the analyte (fluorescent HSA) in the centre line of different cross-sectional sites (positions indicated) compared to the modelled concentration distributions (right) in the mixer structures: a. T-mixer, b. T-mixer staggered blocks, c. herringbone mixer.

Figure 6: The mixing efficiencies of the different structures demonstrated by the square of the relative fluorescent intensity deviation from the average value recorded on centre-line of the outlet surfaces.

Figure 7: The mixing efficiencies (ME) of the herringbone structures as the function of the ratio of groove depth and primary channel depth calculated by Finite Element Modelling.

Figure 8: PDMS microfluidics (a) successfully bonded and aligned onto the polymer surface of the photonic chip containing the waveguides (b).

Figure 9: The time dependent change of the water contact angle on the activated PI surfaces.

Figure 10: Static water contact angle of the modified PDMS plotted against surfactant concentration.

Figure 11: Capillary pressure in the modified PDMS microchannels plotted against surfactant concentration. Values are calculated from the measured contact angles.

Figure 12: Fluorescent intensity change in the microchannel recorded after FITC labelled HSA solution (0.1mg/mL HSA in PBS) injected and washed by PBS. Decreased protein absorption achieved when the original PDMS (a.) modified by 0.2v/v% TX-100 (b.) and 0.2%v/v PDMS-PEO (c.) additives.

Figure 1
Click here to download high resolution image

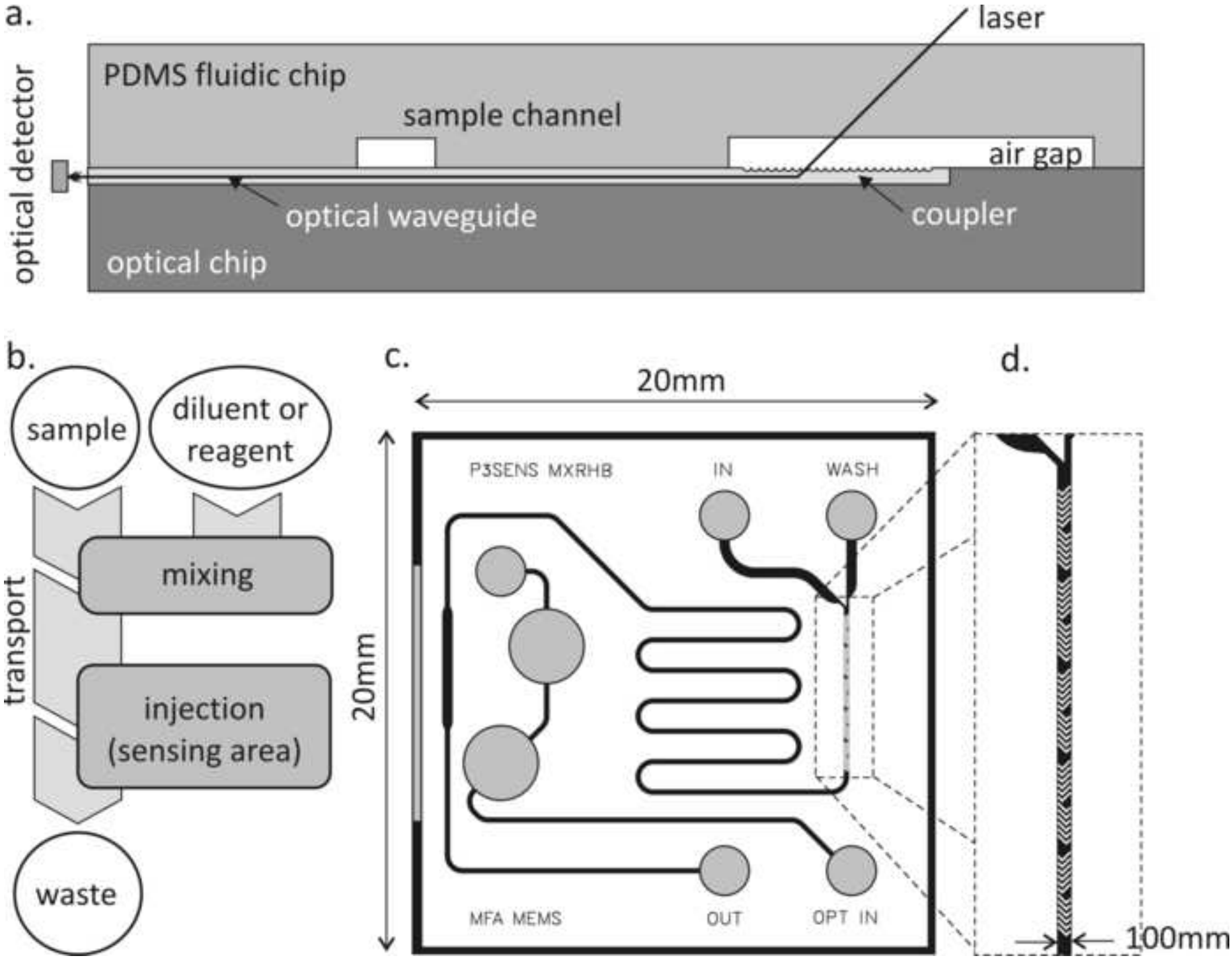

Figure 2
Click here to download high resolution image

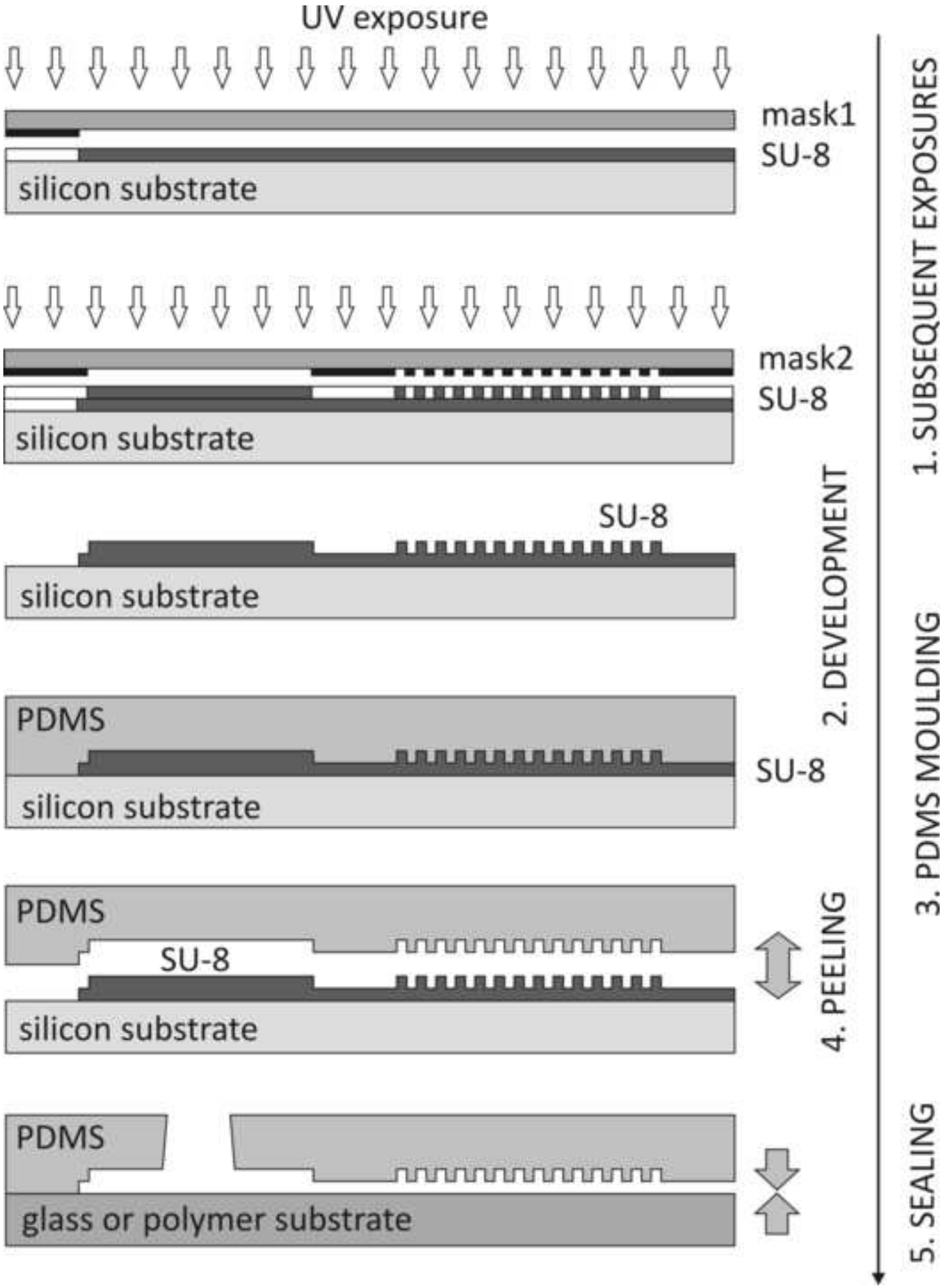

Figure 3
Click here to download high resolution image

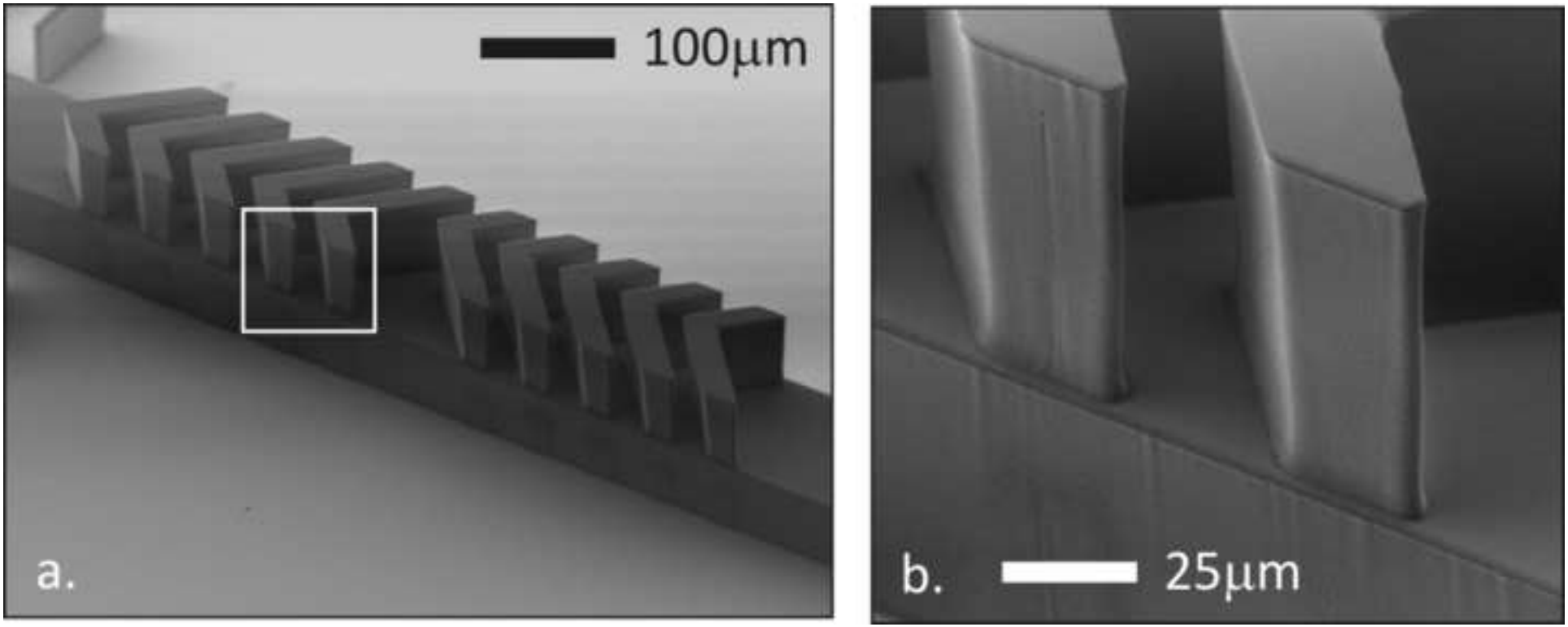

Figure 4
Click here to download high resolution image

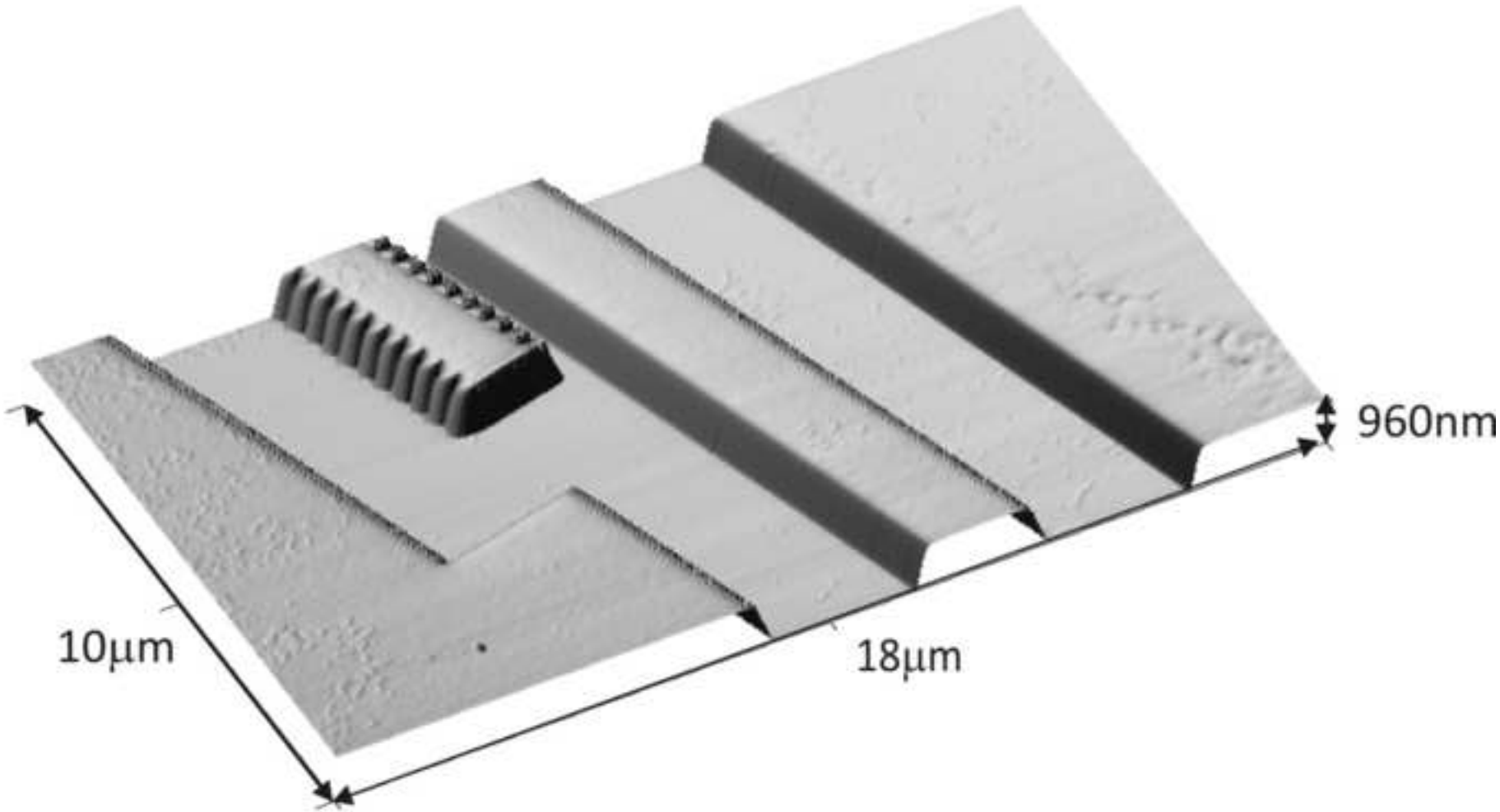

Figure 5

Click here to download high resolution image

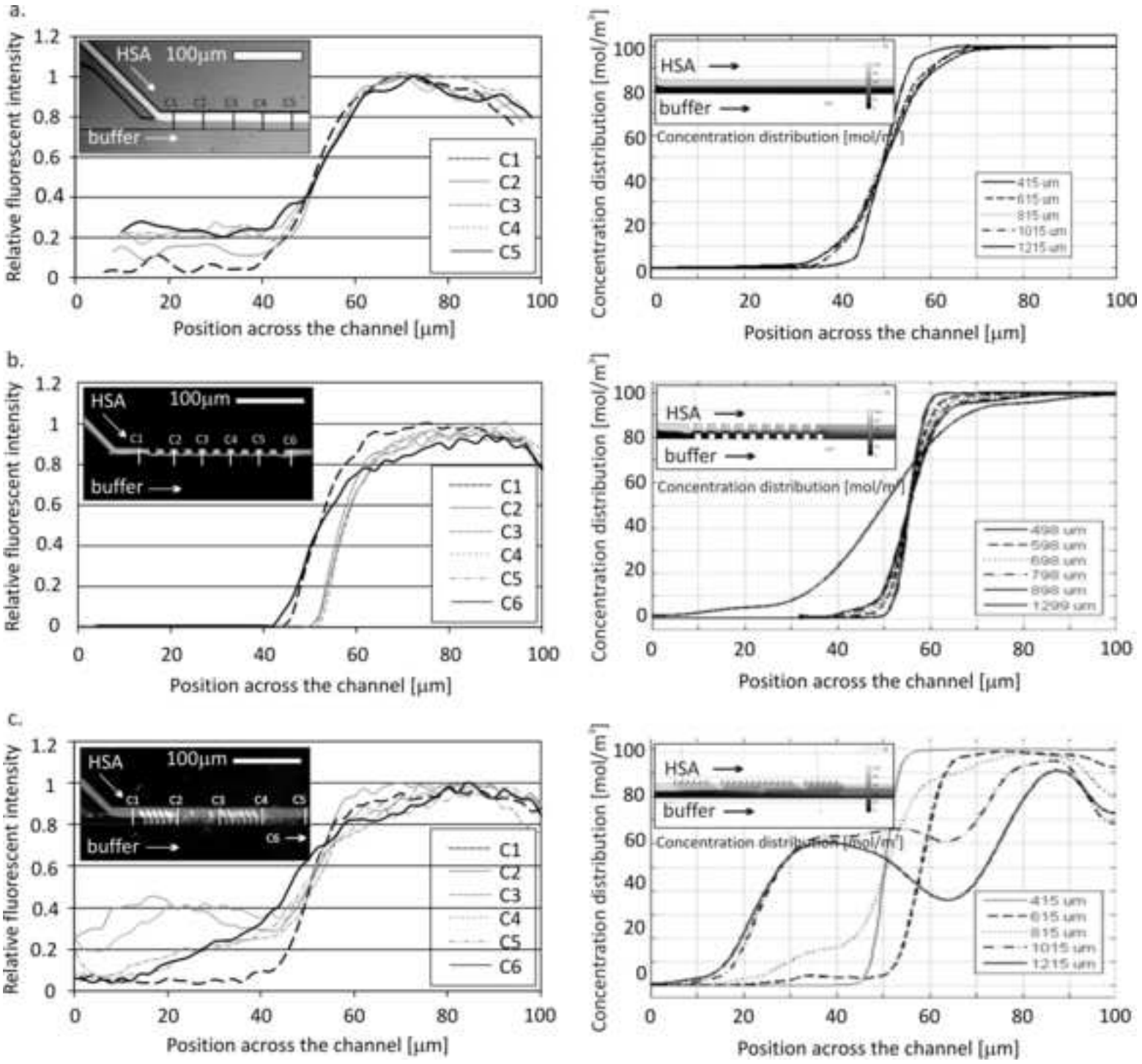

Figure 6
Click here to download high resolution image

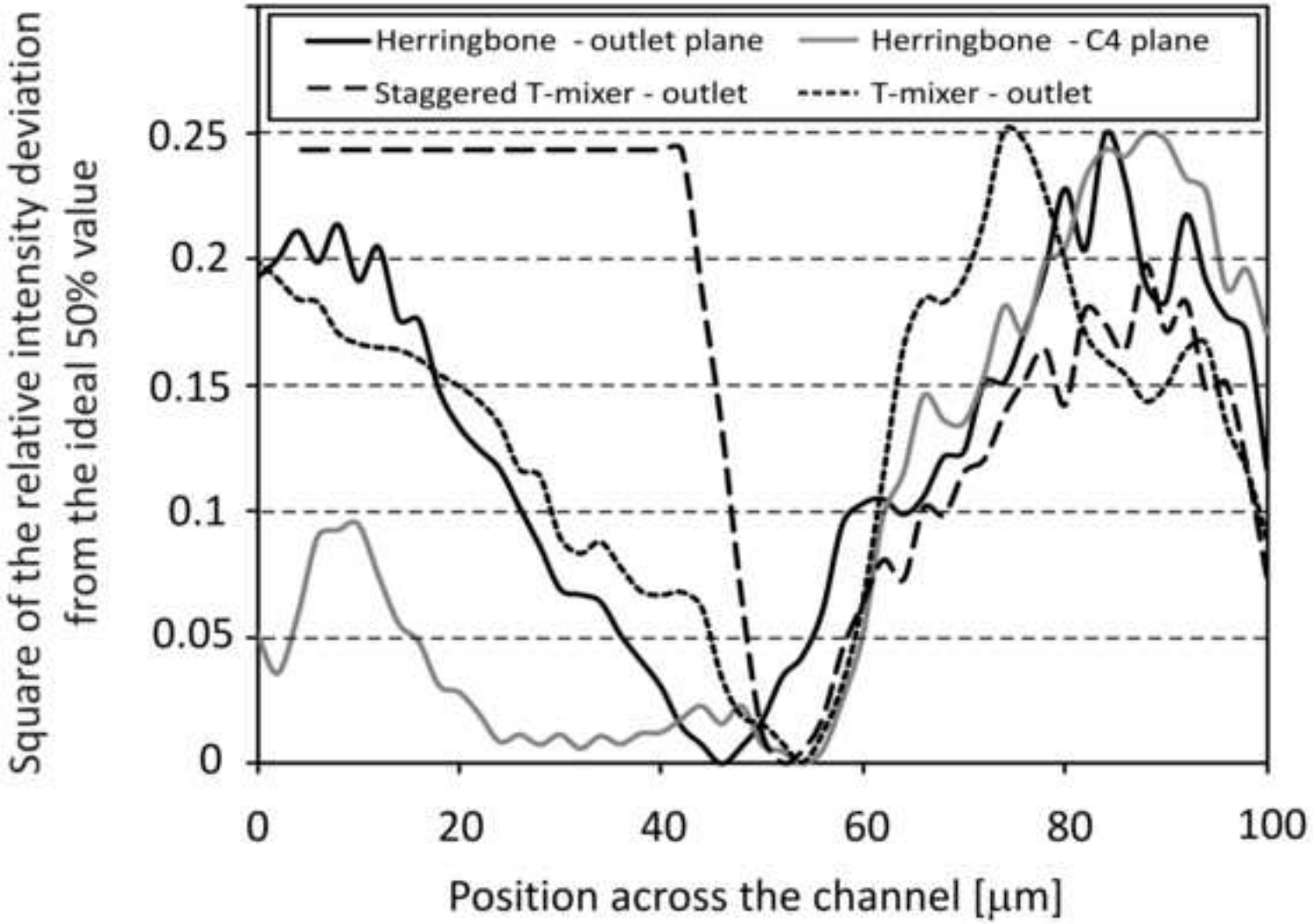

	T-mixer outlet	Staggered T outlet	Herring-Bone outlet	Herring-Bone C4
ME	0.137	0.166	0.128	0.095

Figure 7
Click here to download high resolution image

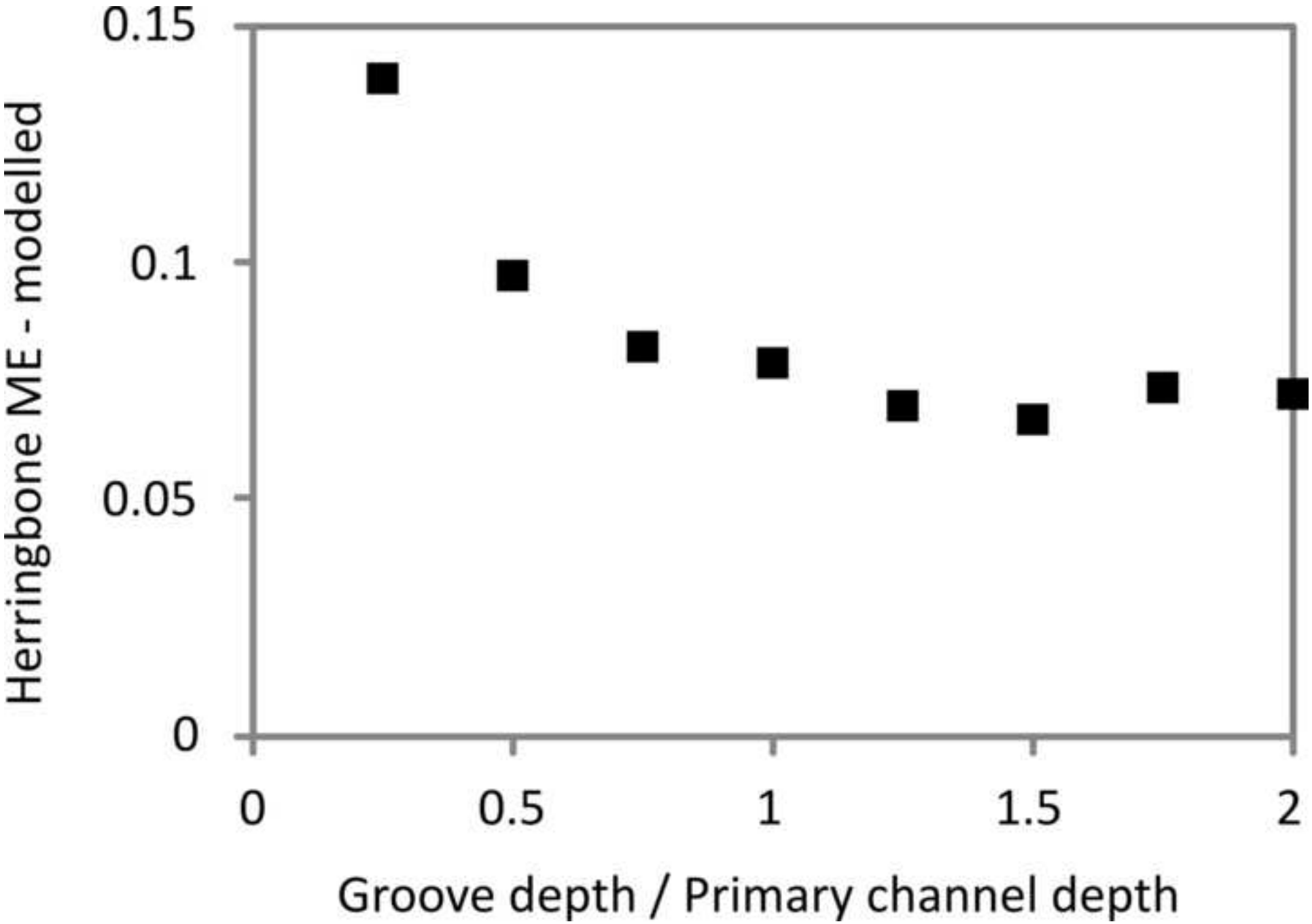

Figure 8
Click here to download high resolution image

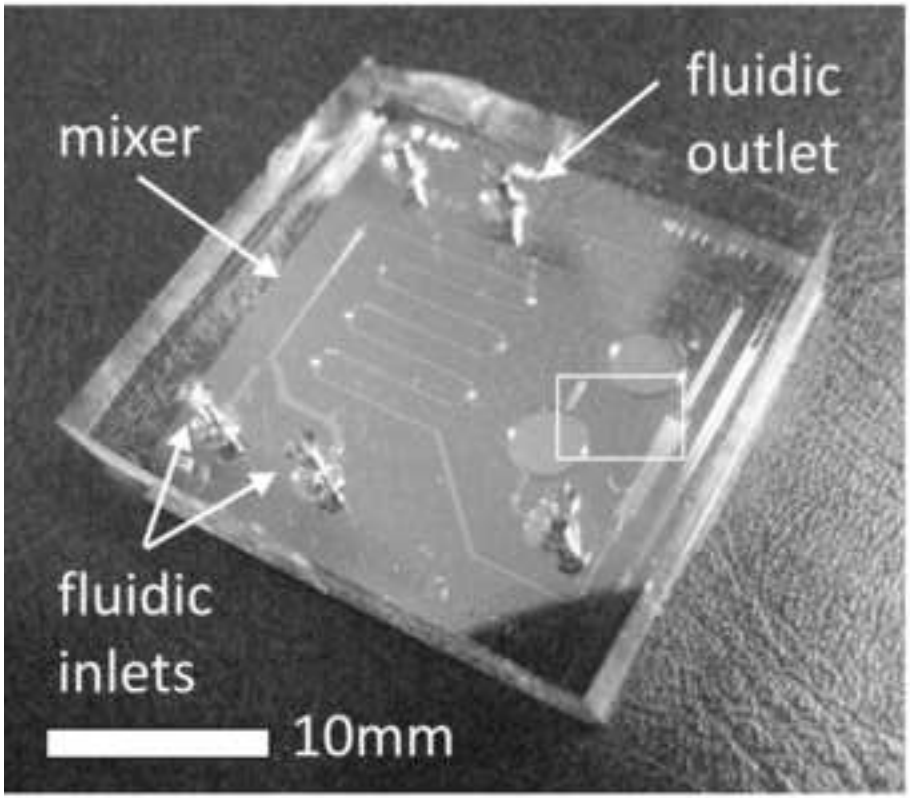

a.

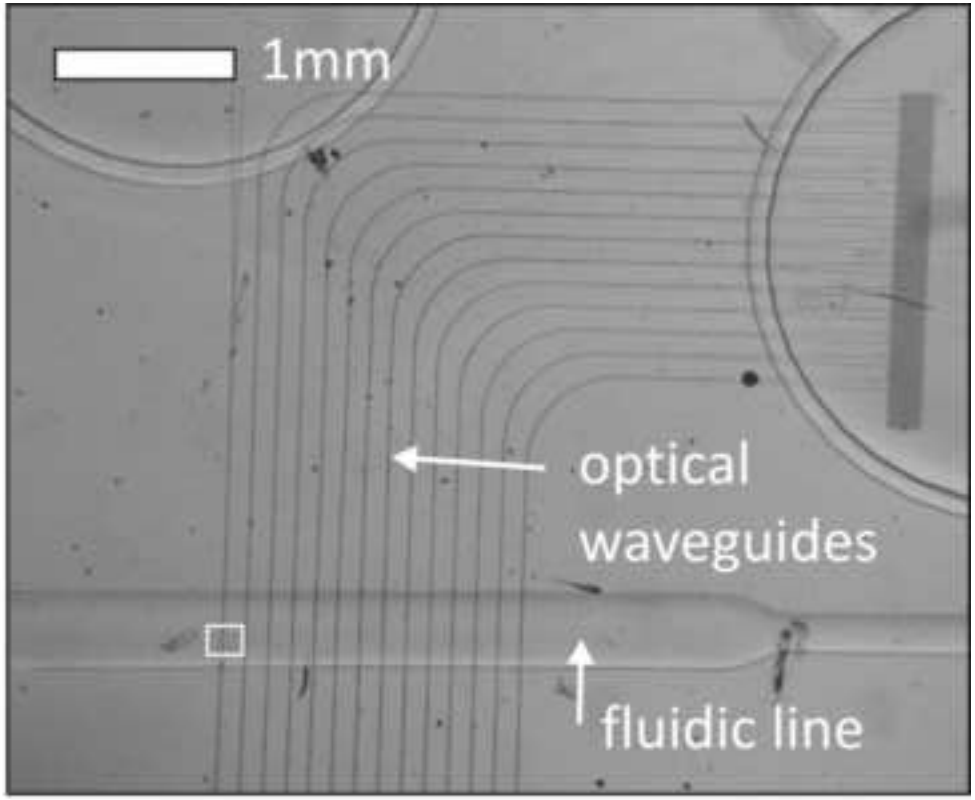

b.

Figure 9
Click here to download high resolution image

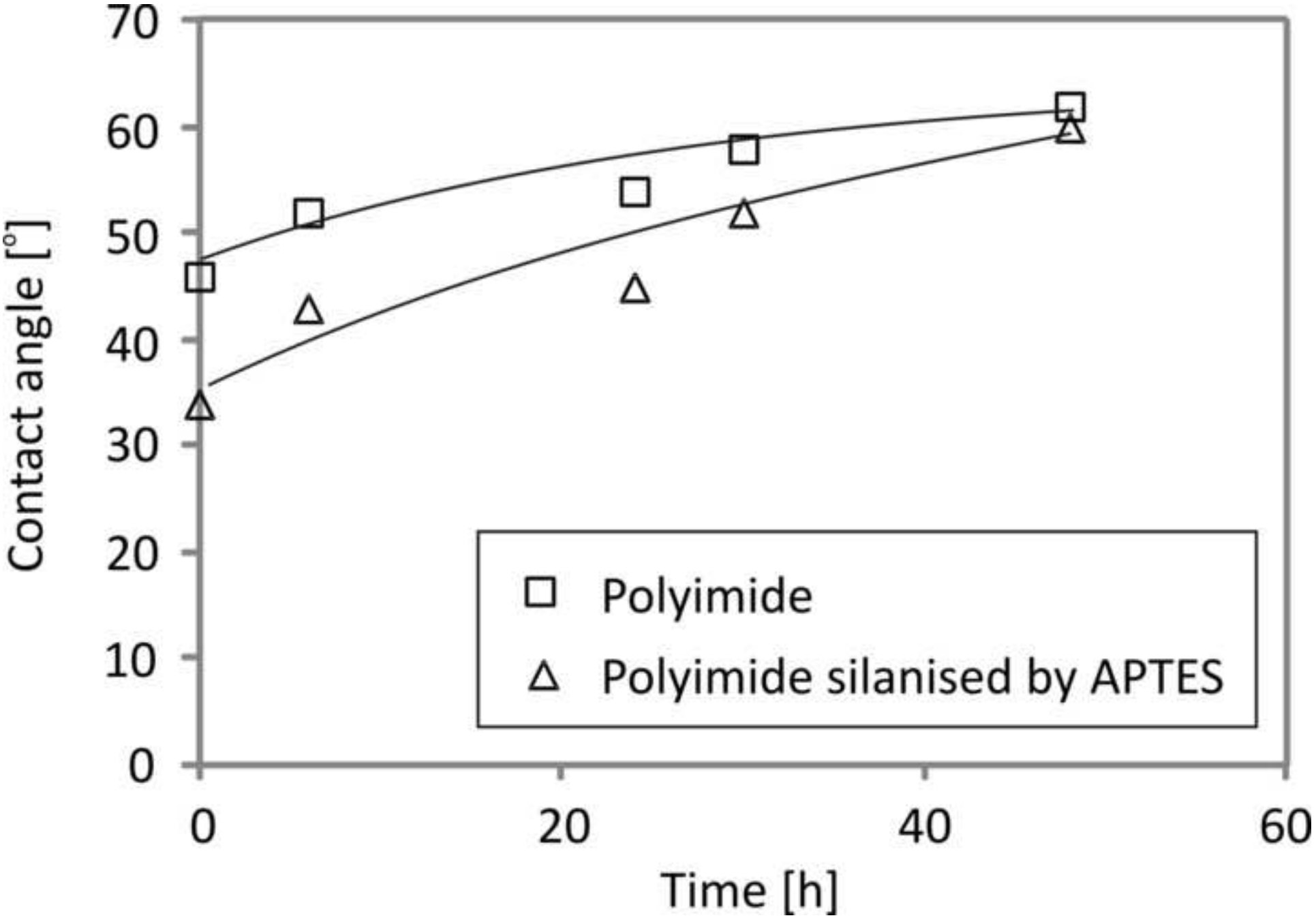

Figure 10
Click here to download high resolution image

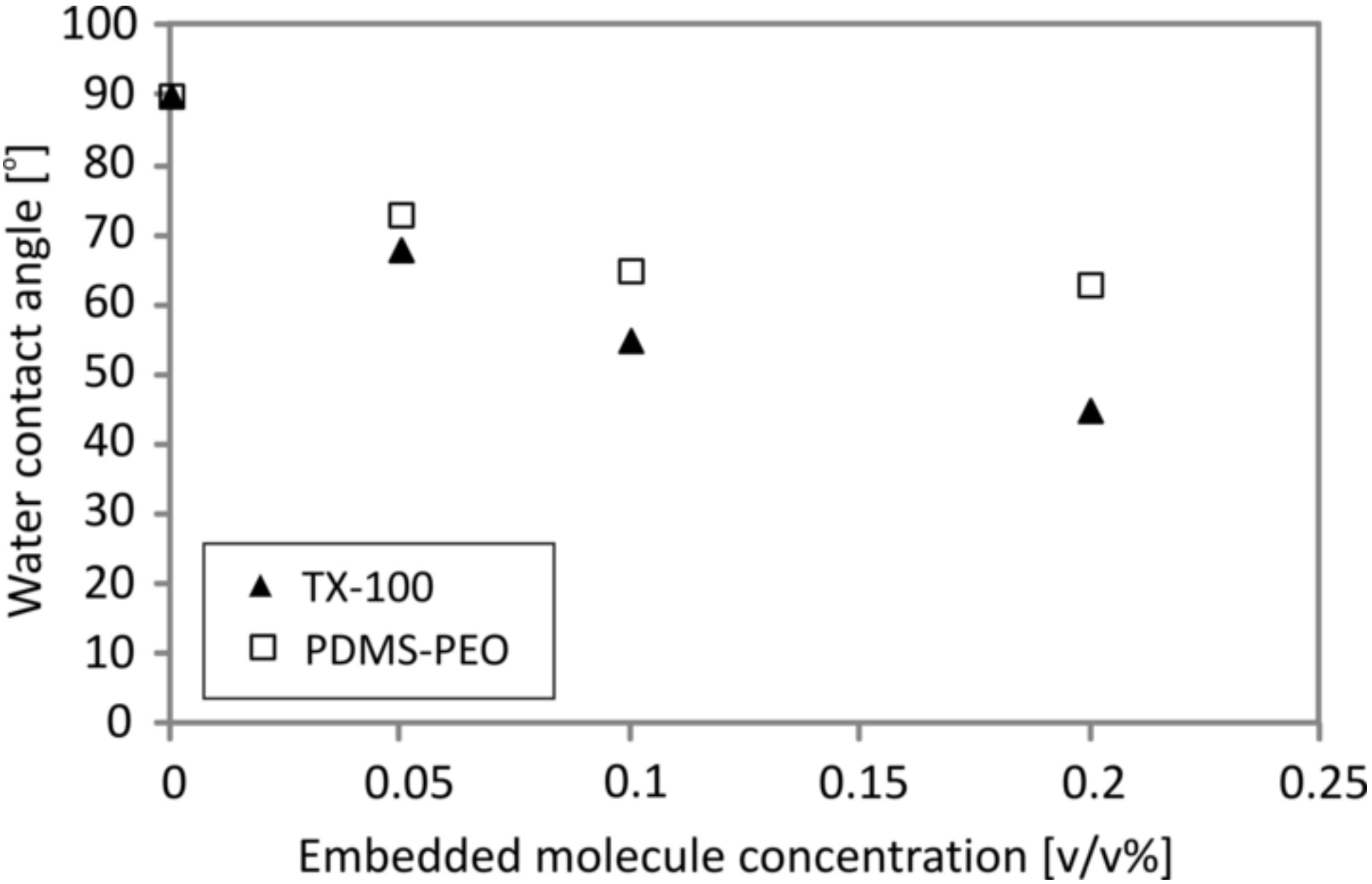

Figure 11
Click here to download high resolution image

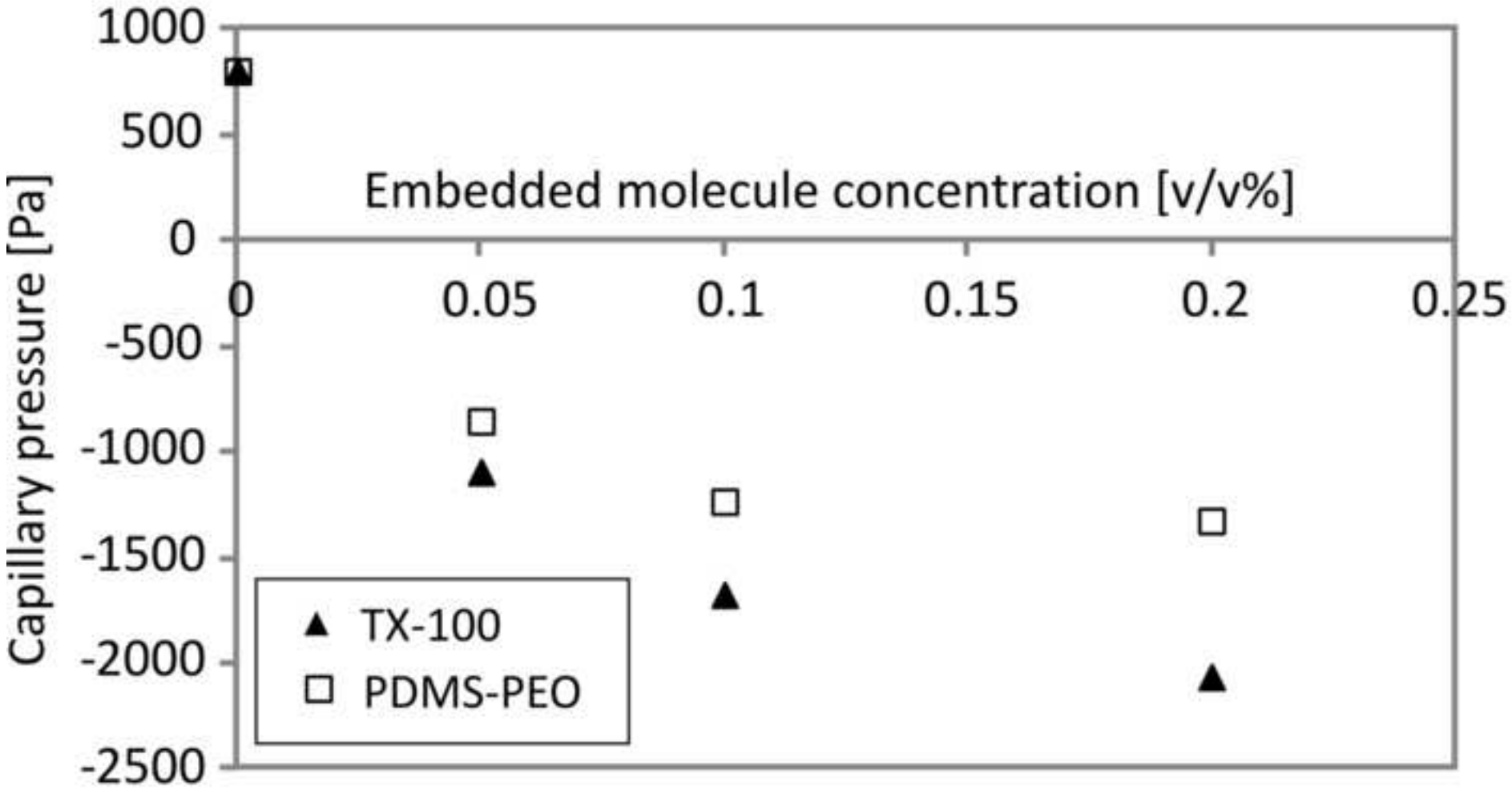

Figure 12
Click here to download high resolution image

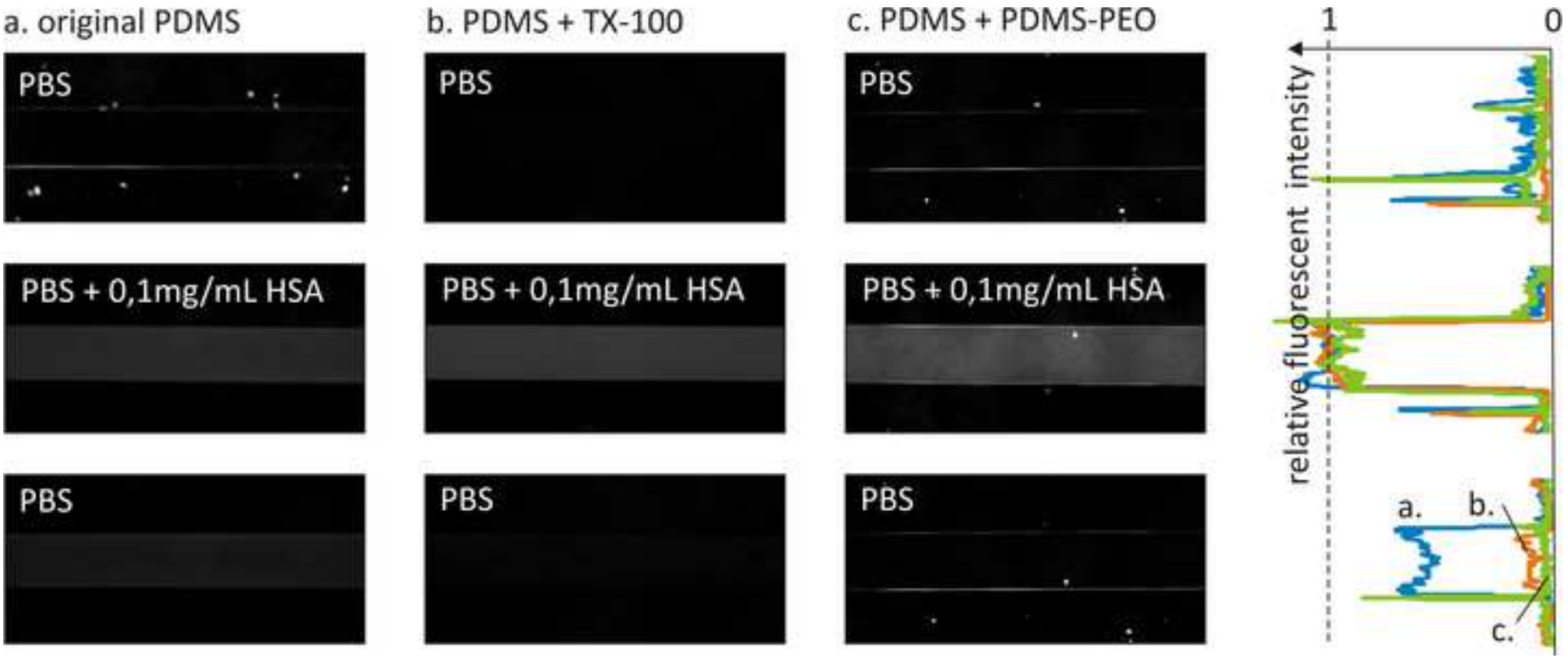

Table 1
Click here to download high resolution image

Applied solution	Injection time	Flow rate
PBS	120sec	2 μL/sec
FITC-HSA (0.1mg/mL in PBS)	30sec	2 μL/sec
PBS	120sec	2 μL/sec

Letter to Editor

Click here to download Attachment to Manuscript: MITE_2013_P3S_Lettertoditor_v2.pdf

Click here to view linked References